Evaluating Performance and Cycle Life Improvements in the Latest Generations of Prismatic Lithium-Ion Batteries

Pontus Svens, Alexander J. Smith, Jens Groot, Matthew J. Lacey, Göran Lindbergh, and Rakel Wreland Lindström

***Abstract*— During the last decade, the market interest for electrified vehicles has increased considerably alongside global climate initiatives. This has coincided with vast improvements in automotive-grade, lithium-ion battery performance. This has increased the range of battery electric vehicles and plug-in hybrids, but lifetime remains a challenge. Aging during fast charging is especially difficult to understand due to its nonlinear dependence on charge rate, state-of-charge, and temperature. We present results from fast charging of several energy-optimized, prismatic lithium-ion battery cell generations with a nickel manganese cobalt (NMC)/graphite chemistry through comparison of capacity retention, resistance, and *dQ/dV* analysis. Changes in cell design have increased energy density by almost 50% over six years of cell development and acceptable cycle life can be expected, even under fast charging, when restricting the usage of the available capacity. Even though this approach reduces the useable energy density of a battery system, this tradeoff could still be acceptable for vehicle applications where conventional overnight charging is not possible. The tested cell format has been used for a decade in electrified vehicles. The ongoing development and improvement of this cell format by several cell manufacturers suggests that it will continue to be a good choice for future vehicles.**

***Index Terms*— Aging, electric vehicles (EVs), fast charging, lithium-ion batteries, Verband der Automobilindustrie (VDA) PHEV2 battery cells.**

I. Introduction

ELECTRIFIED vehicles, such as hybrid electric vehicles (HEVs), plug-in HEVs (PHEVs), battery electric vehicles (BEVs), and fuel cell electric vehicles (FCEVs), are now established on the market. The powertrain technology has been proven for both passenger cars and commercial vehicles such as buses and trucks, despite relatively high component costs when compared to conventional vehicles. Despite very rapid development in terms of increasing energy density and decreasing cell cost, the battery remains the critical component in electric vehicles (EVs) when evaluating total cost, service life, and performance. In order to improve battery system design and usage and develop better estimates for state-of-health, the automotive industry often tests batteries using accelerated aging protocols.

The Swedish automotive industry and several universities have, within continuous research collaboration, carried out a number of studies on aging of automotive-grade Li-ion battery cells, through cycling and postmortem analysis. In its first phase, this collaboration focused on lithium iron phosphate (LFP)/graphite cylindrical battery cells and showed that aging may be severely nonuniformly distributed within battery cells, especially when subjected to high charge rates. This distribution was observed both laterally across the jelly roll surface [1] and throughout the depth of the electrodes [2]. In this cell type, the graphite electrode was particularly affected by severe aging [1], [2]. The uneven aging was argued to be a consequence of inhomogeneous current distribution due to the tab positions, as well as internal variations in temperature, electrolyte wetting, and pressure.

The trend in automotive favors larger prismatic cells, which presents several implicit advantages over small, cylindrical lithium-ion battery cells such as the 18 650 and 21 700 formats, despite the impressive development of new cylindrical cell designs. Prismatic cells offer a better packaging efficiency at system level due in part to fewer connectors and busbars. On cell level, the theoretical packaging efficiency is also higher for large prismatic cells due to the reduced need for passive material, e.g., casing material, pressure relief vents, and terminals. Prismatic cells with stacked electrodes should have more uniform current distribution and internal pressure, which should be beneficial for cycle life compared to cylindrical cells and older prismatic cells where the electrodes are wound in a jellyroll. Cycle aging of large-format cells has been seldom studied in the past, probably due to the high cost and scarce availability of this type of automotive-grade cells.

In the second phase of the Swedish research collaboration, the aging effects of fast charging on such cells were studied. Fast charging capability is widely desired for both passenger cars and commercial vehicles, so a detailed study

Manuscript received 15 September 2021; revised 3 December 2021 and 15 February 2022; accepted 2 March 2022. Date of publication 11 March 2022; date of current version 2 August 2022. This work was supported in part by the Swedish Environmental Protection Agency, in part by the Swedish Energy Agency, in part by the Swedish Electromobility Centre, in part by the VOLVO Group and Scania CV AB, and in part by the Swedish Governmental Initiative STandUP for Energy. *(Corresponding author: Pontus Svens.)*

Pontus Svens is with the KTH Royal Institute of Technology, 100 44 Stockholm, Sweden, and also with Scania CV AB, 151 87 Södertälje, Sweden (e-mail: ponsvens@kth.se).

Alexander J. Smith, Göran Lindbergh, and Rakel Wreland Lindström are with the KTH Royal Institute of Technology, 100 44 Stockholm, Sweden.

Jens Groot is with Polestar Performance AB, 418 78 Gothenburg, Sweden.

Matthew J. Lacey is with Scania CV AB, 151 87 Södertälje, Sweden.

Digital Object Identifier 10.1109/TTE.2022.3158838

was made on one early generation, lithium nickel manganese cobalt oxide (NMC111)/graphite, and prismatic cell type from 2012; in this study, these cells are named type A. From careful postmortem analysis, it was concluded that different aging mechanisms dominate, depending on the charging rate [3]. A parallel study on cylindrical cells of similar chemistry [4] used online mass spectrometry to correlate rapid aging during fast charging with the evolution of large quantities of ethylene gas from electrolyte degradation. Some related works on large, automotive-grade, prismatic cells have recently been published. Gailani *et al.* [5] studied the aging of a large-format, prismatic, NMC111/graphite cell under 1C and 2C cycling. Olofsson *et al.* [6] evaluated capacity loss and impedance change on similar cells containing also NMC lithium manganese oxide (NMC-LMO/graphite) when charged at 2C and discharged using a duty cycle derived from a realistic PHEV velocity profile [6]. Furthermore, Schmitt *et al.* [7] studied pressure increases in large-format prismatic NMC/graphite cells during cycling and Bessman *et al.* [8] compared aging effects with and without a superimposed ac-ripple. Epding *et al.* [9] investigated the capacity recovery observed during rest. Waldmann *et al.* [11] compared the performance of NMC622/graphite cells in the formats prismatic PHEV1 (173 mm × 21 mm × 85 mm [10]), pouch, and cylindrical (21 700); however, these cells were produced in small scale and not intended for usage in automotive applications. At last, Schaltz *et al.* [12] developed a partial charging method for estimating state-of-health of battery cells. The method was applied on both cycle and calendar aged automotive-grade prismatic NMC111/graphite cells [12]. Each of these previous studies limited the charging to 2C at most (corresponding to a full charge in 30 min). From all research efforts, it is well known that Li-ion battery cells experience aging, i.e., loss of capacity and power, during both storage (calendar aging) and usage (cycle aging) due to several mechanisms, each with reaction rates strongly dependent on operating conditions such as temperature, state-of-charge (SOC), charge/discharge currents, and load cycle characteristics. In addition, many of the aging mechanisms are interdependent. The charge rate can in many cases be regarded as the dominant aging factor, especially for energy-optimized cells cycled within large SOC windows, as are typical for EVs and PHEVs.

In this work, we extend our first work on automotive-grade, NMC111/graphite cells and compare performance, reliability, and possibilities for aging analysis with two later cell generations having the same chemistry. We report results for a unique aging protocol that complements prior work in the field. Specifically, cells have been aged by cycling in a limited window (20%–80% SOC) and at elevated temperature (35 °C) using two fast charging currents: 1C and 3C (60 and 20 min, respectively). The data have been acquired by the research consortium over the course of several years. The comparisons here emphasize the progress between the different generations of energy-optimized cells in terms of capacity retention, as well as corresponding internal resistance and incremental capacity (dQ/dV) analyses. By comparing select cells with the same external geometry and active material chemistry, we highlight the effects of the more subtle design changes in recent years. These observations do indeed reflect the clear industry trends of improved energy density and cell lifetime, but we show that those gains: 1) are not always linear; 2) come at the cost of cell densification and heavier packs; and 3) make certain aging metrics obsolete. We suggest the implications of these developments for future cell generations, including preliminary comparison with a nickel-rich NMC811/graphite cell type cycled within the present third phase of the Swedish automotive industry/academy collaboration and a projection to the future performance limits of the PHEV2 prismatic cell format.

TABLE I
SUMMARIZED INFORMATION ABOUT CELL TYPES

Cell type	Market introduction	Capacity (Ah)	Voltage range (V)	Max. rated charge
A	2012	25	3.00 – 4.10	1C
B	2014	28	2.80 – 4.15	1C
C	2016	37	3.00 – 4.20	1C
D	2018	49	3.00 – 4.20	1.5C

II. EXPERIMENT

Three different types of prismatic battery cells of the Verband der Automobilindustrie (VDA) PHEV2 format (148 mm × 26.5 mm × 91 mm [10]) were cycled at the same temperature, +35 °C measured at the tabs, and in the same SOC region. The electrode active material was NMC111/graphite for the three tested cell types. Cycling was done in a 20%–80% SOC window, with constant charge and discharge currents without resting time between charge and discharge. The charge and discharge time required to stay in the SOC window was recalculated every 200th cycle from periodically performed capacity measurements and was hence based on a Coulomb counting method. In addition to the periodic capacity measurements, direct current internal resistance (DCIR) measurements were performed, followed by constant voltage adjustment to 80% SOC before the next cycling period. The periodically performed tests consisted of $C/4$ discharge capacity measurements between the upper and lower voltage limits for each cell type, as described in Table I, as well as DCIR measurements at 50% SOC, which consisted of a 50-A discharge pulse for 18 s applied after 1 h of rest. The DCIR was calculated as the ratio between the voltage drop and the applied current, after 2 ms into the discharge pulse. Two cells of each cell type were cycled at 1C/1C (charge/discharge) current and two cells per cell type at 3C/1C. Cycling of cell types A and B was done on Project Engineering and Contracting (PEC) SBT0550 equipment from PEC Products N. V. Additional information about all cell types is shown in Table I.

For cell type C, reference cells were also stored in different temperatures during the testing period in order to measure the calendar aging separately. The conditions for the cell cycling and reference performance testing of cell types A and B, which were cycled at the same test facility, are described in detail in previous work [3]. The cycling of cell

type C was done at another test facility under the following conditions. Cycling and performance testing were done on a Maccor Series 4000 cell tester. All cells were placed in a climate chamber operating at an average temperature of +33 °C ± 1 °C during testing to obtain the same average cell tab temperature of +35 °C (measured individually with surface-mounted thermocouples) as cell types A and B. Steel plates were attached to all cells during cycling to maintain external cell pressure according to supplier recommendation. The applied test protocol was the same as for cell types A and B. One additional cell type, called D, in the same format but with the nickel-rich electrode active material NMC811, is used as a reference but was not included in the original test matrix. This cell type has been cycled under other conditions and detailed results from that work will be published separately.

III. Results

In this study, three different generations of prismatic NMC111/graphite cells are compared from 2012 (A), 2014 (B), and 2016 (C). We build on our previous publication on cell type A and present a comparison due to performance improvements over recent years. We also discuss relevance of certain techniques for estimation of aging, capacity, and power from cycling data and simple *in situ* tests. Finally, we reflect on the implications of battery behavior and analysis for the electrification of heavy-duty vehicles.

The designs of the cells are shown as X-ray images in Fig. 1. Despite having the same external dimensions, they have different internal configurations. Type A has a single jellyroll with the current collector tabs oriented to the short side (vertical winding). Type B has two jellyrolls in the same direction as A, making better use of the cell can volume. Type C retains the double jellyroll design but with the tabs facing the longer side instead (horizontal winding), further improving the use of the cell can volume.

A. Capacity Retention and Coulombic Efficiency

The effective lifetime of the cells can be discussed as their cyclability or the number of cycles to reach 80% of the initial capacity. As expected, significant improvement is registered between the generations and can be seen in the capacity retention curves versus equivalent cycles in Fig. 2. Generally, all cells experience a steeper decline in capacity with faster charging [3C in Fig. 2(b)]. The improvement between generations is more apparent at 1C than at 3C. The dependence on C-rate on aging for cell A was investigated in depth in our previous article [3]. While NMC particle cracking was observed at 1C and 2C charging rates, lithium plating likely reduced lifetime at 3C charging rate, and gas evolution rapidly killed the cells cycled with 4C charging rate. Even for NMC111/graphite cells, heterogeneous aging within the cell was observed. For instance, a difference in DCIR was observed among samples harvested from the curved and the flat regions of the prismatic cell jelly roll, suggesting a nonuniform distribution of mechanical pressure affecting the local aging [13].

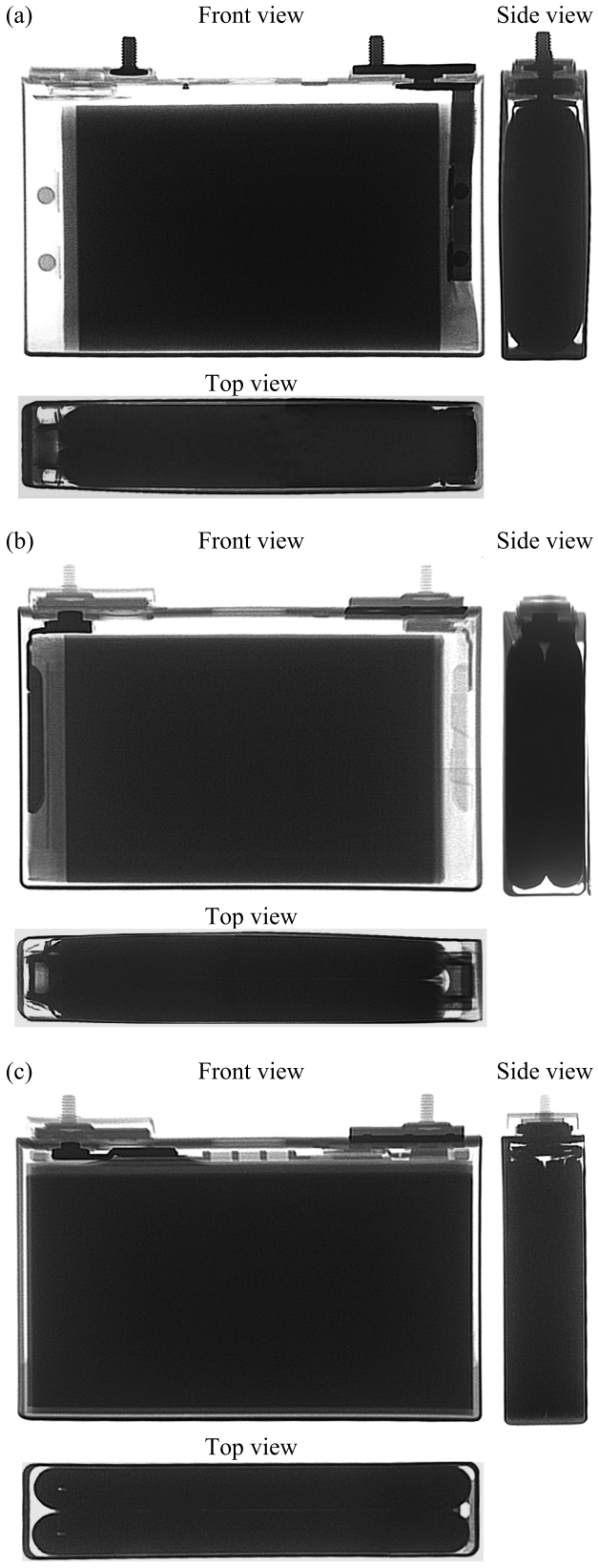

Fig. 1. X-ray images (front, side, and top views) of cell types (a) A, (b) B, and (c) C.

Fig. 3 includes the complete capacity retention curve for each cycled cell and shows good agreement among the duplicate cells. Cell type B has the greatest spread between cells at 3C charging, which could be related to tolerances

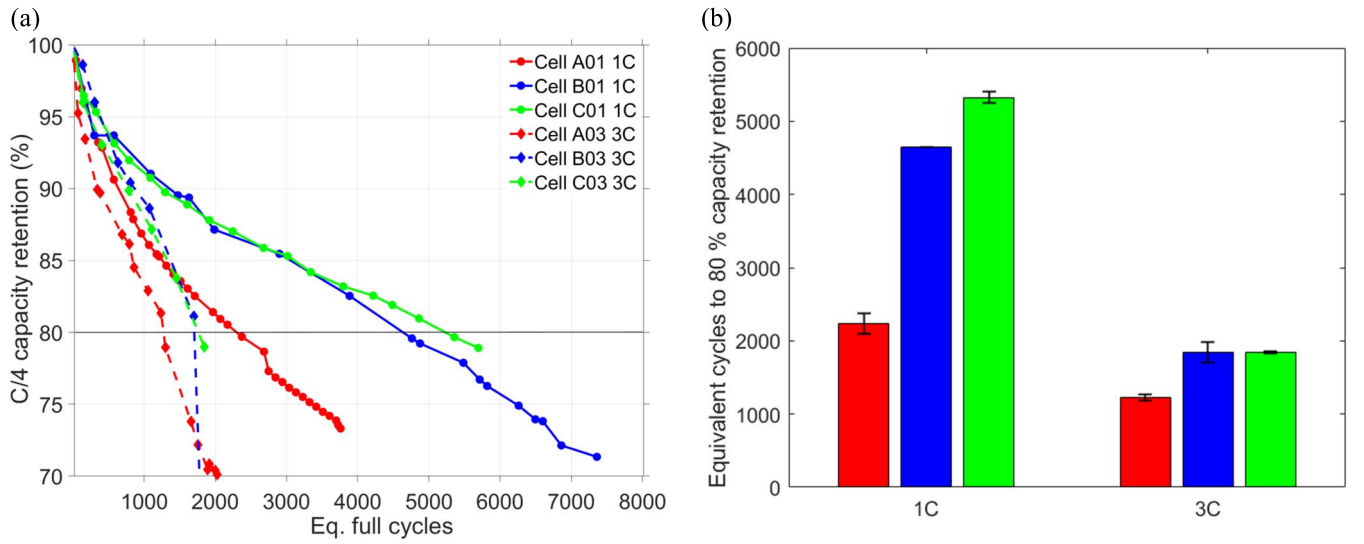

Fig. 2. Capacity fade for all cycled cells at the two charging currents used, depicted as (a), capacity retention versus equivalent full cycles and (b) equivalent cycles at 80% capacity retention versus charging current. The error bars in (b) show the spread between duplicate cells within the different test pairs.

in cell manufacturing or sensitivity to slight variations in test conditions. The measurement of coulombic efficiency (CE, high-precision measurement of the losses between each charge and discharge step) is a common tool for analyzing aging [14]. The relationship between CE, the capacity retention, Q, and the number of equivalent full cycles, N_{eq}, can be described by the following equation:

$$Q = (\text{CE})^{N_{\text{eq}}}.$$

The CE can be estimated from the shape of the retention curve, as shown in Fig. 3, for different stages of aging fitted with solid, dashed, and dotted black curves representing the calculated capacity retention assuming periods of constant CE. This fitting can be used as a retroactive and semiquantitative indicator of the aging rate and periods of accelerated or decelerated aging dependent on cell and use conditions can be identified.

Using this approach, we achieve a good visual fit with three consecutive CE slopes for the capacity retention at 1C charge current [Fig. 3(a), (c), and (e)]. All cell types experience an increasing CE under 1C charging, hence showing a regressive or decelerating aging behavior beginning after a couple of 100 equivalent full cycles. Cell type B appears to have a slight decrease in CE near end of life (EOL). The capacity retention for cell types A and C can be fitted with a single CE curve for the 3C charging case [Fig. 3(b) and (f)]. The estimated CE, in this case, is similar to the estimated CE1 for the corresponding cells charged at 1C. A similar behavior is also seen for cell type B under 3C charge; its fitted CE-curve also has an efficiency corresponding to the first fitted CE curve for the 1C cycled cells. However, in this case, there is also a sudden change in slope at around 80% remaining capacity, where the estimated CE decreases drastically [CE2 in Fig. 3(d)]. In summary, aging decelerates using the 1C charge strategy but remains constant (or even accelerates near EOL) for the cells cycled with the 3C charge strategy.

Common for all three cell types is that 3C charging rates result in lower cyclability relative to 1C charging rates. The largest difference can be seen for cell type C that only shows around one-third of the cycle life at 3C charging compared to 1C charging. All cycled cells also showed swelling at end of testing, especially cells cycled at high charge C-rates. Compared to cell tests done at similar test conditions presented in the literature, the cycle life at 1C shows higher values in our case for cell types B and C but generally lower values for cell type A [5], [7], [8]. In addition, for cell type C, a time-dependent aging mechanism was also measured by means of a calendar aging test at 50% SOC. As expected, calendar aging of this type of lithium-ion cell has a capacity loss proportional to the square root of time [15], [16] [see Fig. 3(f), inset]. At an elevated cell temperature of 45 °C, calendar aging effects may contribute up to 6% capacity fade after 1000 days. With cell temperatures maintained below 35 °C, the observed calendar aging effects comprise a minor contribution to the overall aging photograph. At +33 °C, this contribution does not exceed 4% capacity fade after 1000 days, exceeding the span of this cycling study. In our selected temperature window, we, therefore, expect cycle aging effects, as reflected by our CE-fitting strategy, to dominate the observed long-term aging behavior.

B. Correlation Between DCIR and Capacity Retention

DCIR measurements were performed throughout testing with constant current pulses of short duration. The measurements capture information about the changes in electronic and ionic resistances of the cells during cycling. The results shown in Fig. 4 reveal an approximately linear correlation between DCIR and capacity retention throughout cycling for cell type A. However, this trend is not observed for cell types B and C. Both newer generation cell types have a higher DCIR value at the beginning of cycling and reach a DCIR minimum after some 100 equivalent full cycles before the resistance starts to increase. The anomalous behavior of cell C02 [cycled at 1C, Fig. 3(e)] is attributed to an error with the measurement. Its duplicate cell C01 was more stable, demonstrating the more

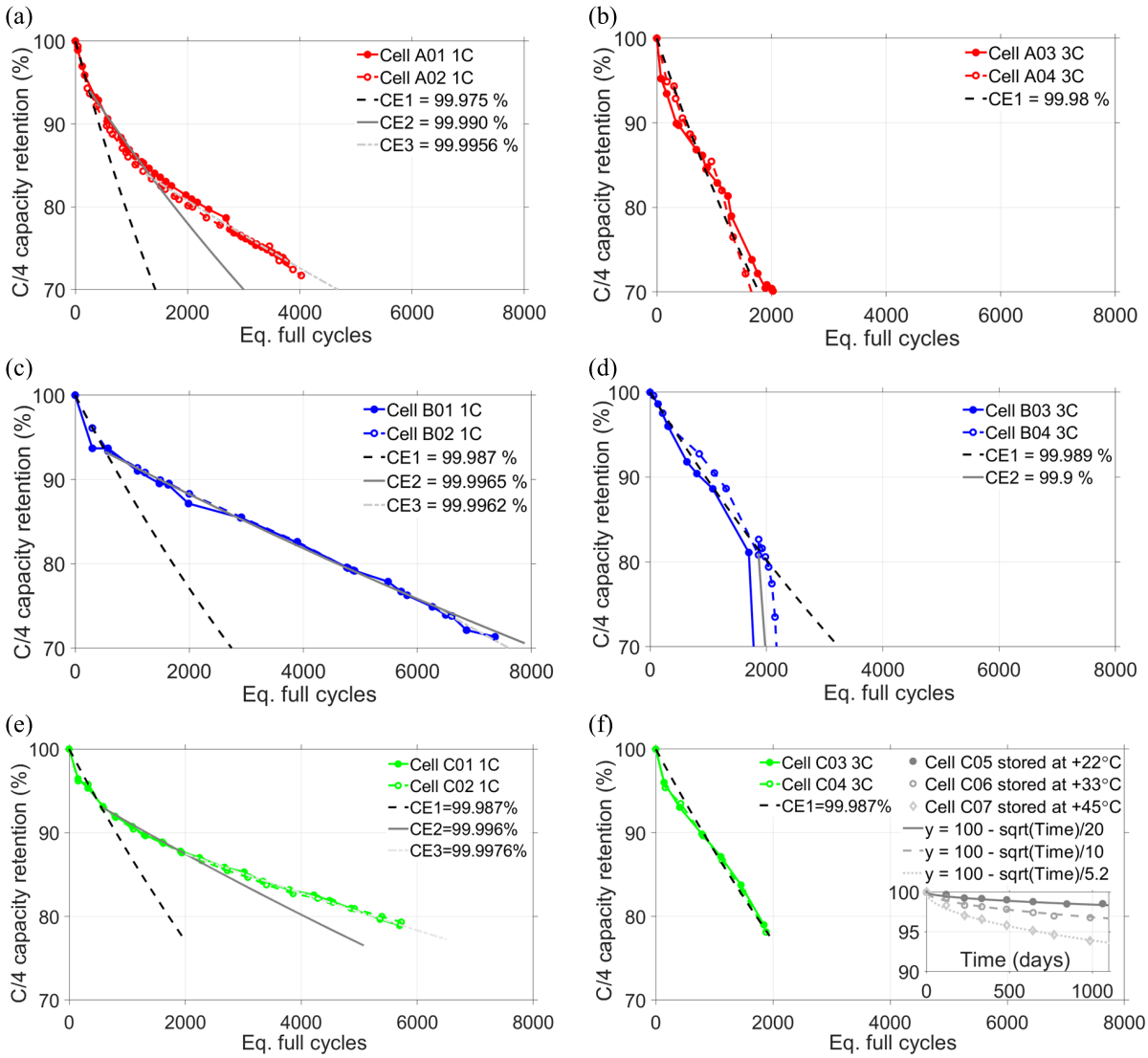

Fig. 3. Observed capacity retention for aging at 35 °C (colored curves) and calculated capacity retention for select values of constant CE (black curves) for (a) cell type A under 1C/1C and (b) 3C/1C cycling, (c) cell type B under 1C/1C and (d) 3C/1C cycling, and (e) cell type C under 1C/1C and (f) 3C/1C cycling, with calendar aging (gray curves) in inset.

regularly observed early-life decrease and late-life increase in DCIR.

An initial decrease in DCIR has also been reported by Gailani *et al.* [5] but is otherwise seldom reported in the literature. The phenomenon could be related to several possible causes, of which one could be variations in the formation process between cell candidates [17]. Recent cell generations have more advanced materials, design, and production, using electrolyte additives or protective layers to stabilize the cell for storage before sale or to prevent aging during cell usage. It is possible that the decrease in DCIR is related to the consumption of these sacrificial additives or some other activation behavior inside the cell such as porosity increase or internal swelling. The latter would lead to increased pressure that could improve internal contact, reducing DCIR during early in life, even though in the long term, these mechanisms contribute to undue stresses and aging. It should be mentioned that cell swelling was observed for all cells at EOL.

The results imply that the direct correlation between capacity retention and DCIR rise is challenging and generally not evident in a real-life vehicle application. From our data, only the older generation cell type A shows such a clear dependency. Evidently, the relationship between DCIR and capacity retention for cell types B and C is not linear, but rather a U-shaped curve with a minimum close to the shift to the constant aging regime noted by the CE estimation. Whether there is a reliable correlation is, however, not possible to say from these data and would require further study. The nonlinear correlation observed in more recent cells makes it considerably more complicated to apply an estimation for battery capacity estimation from DCIR measurements alone in a real-life vehicle application.

C. Qualitative Aging Mode Analysis

Finally, the changes in the negative and positive electrodes were followed using the incremental capacity analysis, i.e., the derivative (dQ/dV) of charge and discharge voltage curves. This method has been demonstrated as a valuable tool to analyze aging [18]. The results are presented for beginning of life (BOL) and EOL in Fig. 5.

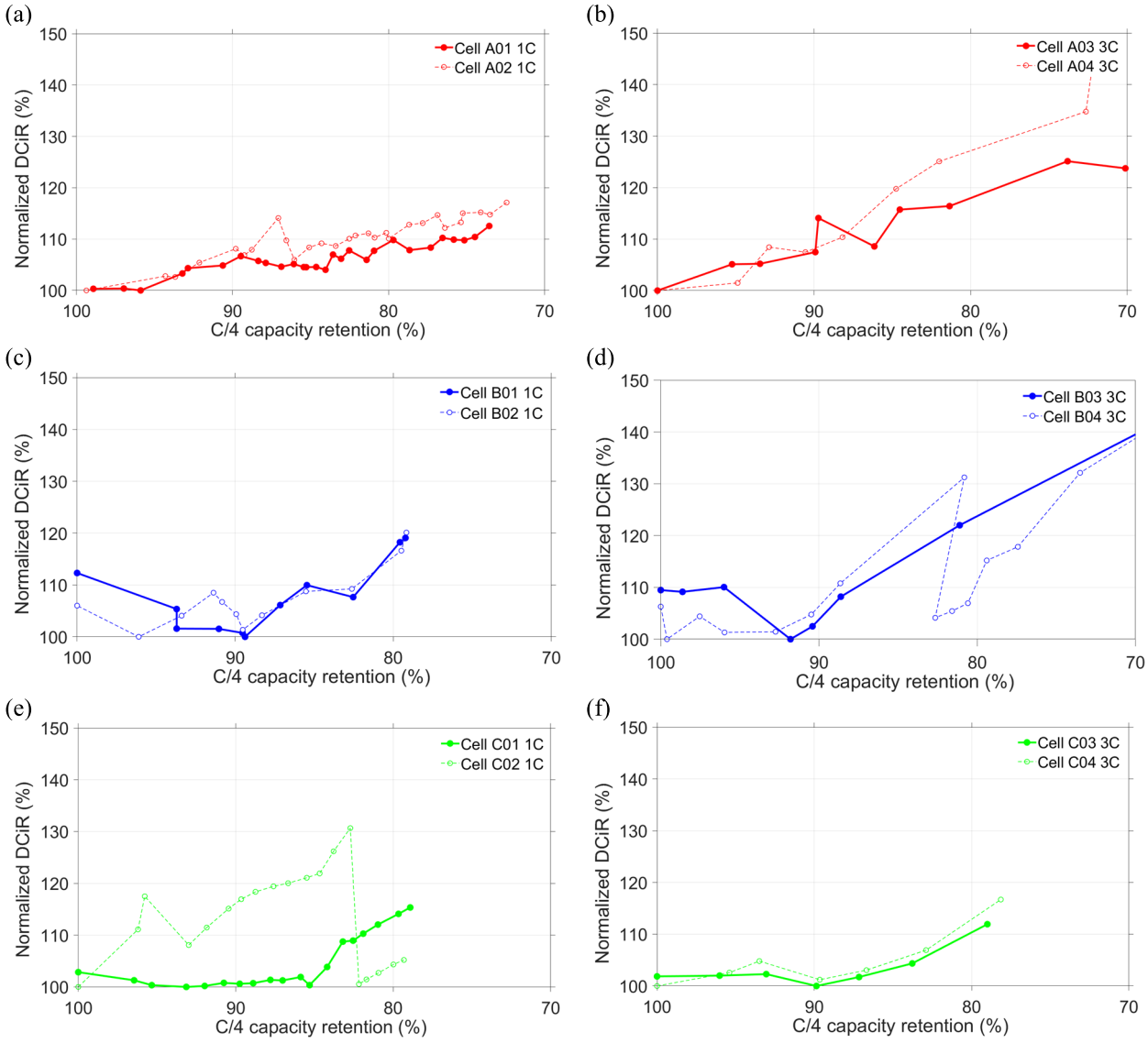

Fig. 4. Correlation between DCIR and capacity retention for cell type A: (a) 1C charged cells and (b) 3C charged cells; for cell type B: (c) 1C charged cells and (d) 3C charged cells; and for cell type C: (e) 1C charged cells and (f) 3C charged cells. DCIR is measured from 2-ms discharge at 50% SOC and normalized to 100% at the minimum value for each cell.

Peaks in *dQ*/*dV* curves relate to phase equilibria of active electrode material (voltage plateaus in voltage versus capacity plots) [19]. For the cell-type NMC111/graphite, two peaks are dominant: one at around 3.5 V mostly related to the negative active electrode material graphite and one at around 3.65 V mostly related to the positive active electrode material NMC111. As expected, the features are similar for all three generations as they use the same electrode active materials.

The shifts and sizes of the peaks are also similar for the cells with a major difference that the first peak at 3.5 V of cell type A after cycling with 1C charge is only shifted and not smeared out at EOL; this shift can indicate loss of cyclable lithium [18], [20]–[23]. However, this peak nearly disappears after cycling with 3C charge. In addition, the second peak at 3.65 V is more diminished for this cell type than for the others at EOL and even more so for the 3C protocol. From these observations, it is clear that cell type A experiences different aging processes dependent on the charge rate. The peak features for cell types B and C experience similar changes independent of the cycle rate. Though extended cyclability remains a challenge, improvements to cell design in the recent cell generations have helped to homogenize the aging processes and improve rate capability.

The loss of peak area around 3.65 V could be related to a loss of NMC active material, as was confirmed for cell type A in our earlier work [3]. However, cursory analysis of the corresponding *dV*/*dQ* curves shows no strong evidence for this in the later generations. Moreover, the capacity attributed to the solid solution behavior of NMC111 at cell voltages above 3.7 V appears to be retained [18], [24]. This capacity is observed as a constant, nonzero *dQ*/*dV* value at high voltage. This implies that while much of the positive electrode material remains intact, it may be incompletely lithiated on discharge due to limitations of the negative electrode, lithium inventory,

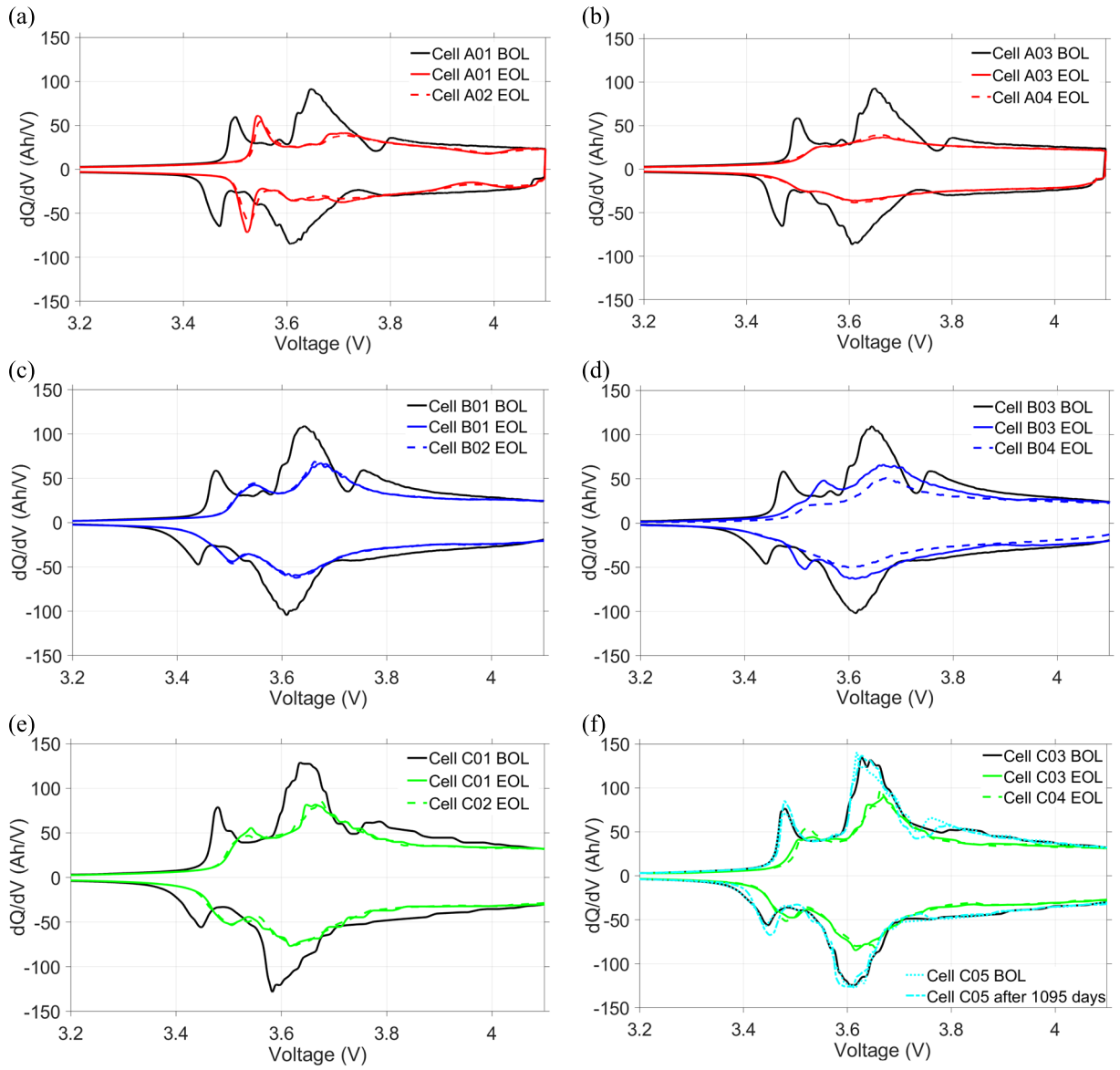

Fig. 5. *dQ/dV* plots for (a) cell type A at 1C charge and (b) 3C charge, (c) cell type B at 1C charge and (d) 3C charge, and (e) cell type C at 1C charge and (f) 3C charge and calendar aged (cyan). Due to high overlap and low variability among cells at BOL, only a single BOL curve is shown for each case.

or other factors. The marked decrease in the low-voltage peak further suggests that loss of graphite active material at the negative electrode may be responsible, alongside loss of cyclable lithium.

The behaviors of cell types B and C are similar and presented together here. For both, 1C and 3C cycled cells alike experience loss of area under both main peaks at EOL. Peak shifts indicating loss of cyclable lithium are observed, alongside a broadening of several peaks, particularly for the negative electrode. The sharp, well-defined peaks at BOL represent the electrochemical reactions in relatively homogenous electrodes. The broadening and smudging of these peaks at EOL indicate the occurrence of these reactions over wider windows of cell voltage. In this way, peak broadening indicates increasing heterogeneity and local gradients of both SOC and overpotential within the cell. Broadening without loss of integrated peak area does not entail loss of capacity. There are no substantial changes in the incremental capacity profile of a calendar aged cell [Fig. 5(f), cyan] after 1095 days of storage, indicative of the very low degree of capacity fade.

IV. Discussion and Summary

The energy density of prismatic lithium-ion battery cells of the PHEV2 VDA-format has increased significantly from their market introduction until the present. Overall, our results indicate that this type of cell could be suitable for applications such as PHEV distribution trucks, where there are demands for zero tail-pipe emissions and silent driving during night delivery. However, to obtain a reasonable lifetime from a corresponding battery pack, the charging rate should be limited to around 1C. For example, a PHEV distribution truck that cycles the battery between 20% and 80% SOC two times per day for 250 days per year should, in the best case, be able to achieve a battery service life of around ten years (until

80% capacity retention), as estimated from the data obtained for cell type C. With a 3C charging regime, this figure would instead be less than four years, which could be challenging for the customer. The development of fuel cells for heavy-duty commercial vehicles has gained renewed interest for hybrid electric drivetrains based on a combination of fuel cells and power-optimized batteries. However, many manufacturers and applications are trending toward more energy-optimized configurations. For such heavy-duty BEV applications where all traction and auxiliary energy needs to come from the battery, a traction battery with very high energy density is needed. In applications where charging can be done during longer periods (<1C), a pure energy-optimized cell type should be a suitable choice. Today, more energy-optimized cells in the PHEV2-size are also available. For example, it has from around 2019 been possible to obtain PHEV2-size cells with around 50 Ah from selected cell suppliers [25]. These cells are typically composed of a nickel-rich NMC positive active electrode material, sometimes in combination with a silicon-containing graphite negative active electrode material to reach high capacity. Looking to the future, from a simple model based on current cell designs, we project that a high-nickel-content cathode combined with a solid-state electrolyte could push future PHEV2 battery cell capacities to near 100 Ah, corresponding to a very high volumetric energy density as well as specific energy (>1000 Wh/L, >350 Wh/kg). Since the trend in automotive electrification increasingly points toward pure BEVs, many battery suppliers are focusing on developing more energy-dense battery cells.

This development in automotive-grade prismatic cells over the course of cell types A (2012), B (2014), C (2016), and beyond is summarized in Fig. 6. While our results may not necessarily be representative of the entire battery industry, we have selected a subset of automotive-grade cells with the same chemistry and form factor in order to show the influences of cell internal design, cell quality, and other engineered factors in the past decade of automotive batteries. Independent of chemistry, these results highlight the vast improvements in performance and reliability that have been achieved in the span of a few years. We caution battery researchers and users to be aware of such differences when comparing and benchmarking results across different periods of battery development.

In addition to the improvement in volumetric energy density throughout cell generations, there is an improvement in specific energy, though this is less pronounced. This means that for each generation of cells produced in this format, more capacity can be fit into the same cell housing, but at a greater weight. This effective densification of the cells has interesting implications for the automotive industry. A battery pack built with a certain size specification in 2018 may deliver about 90% more energy than a visually identical pack built in 2012, but will also be around 30% heavier, assuming a high gravimetric cell-to-pack ratio of 60%. Hence, the same weight of batteries would in 2018 have given a 38% increase in capacity compared to 2012. The impact of this tradeoff between pack energy and pack weight can be far-reaching for mobile applications. Trucks designed with heavier battery packs would, in some cases, have to sacrifice payload in favor of range.

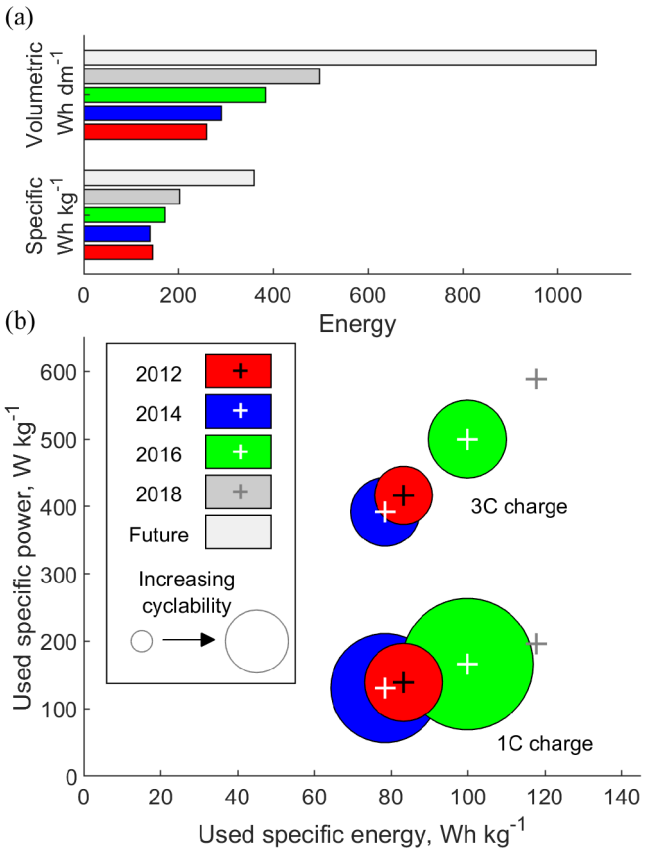

Fig. 6. Evolution of (a) volumetric energy density and nominal specific energy and (b) ENPOLITE-style plot evaluating used specific power, used specific energy, and lifetime as described in [26]. Study of cell type D (2018) and beyond is ongoing and their cyclability is not yet reported.

In order to encourage comparison with other aging studies in the field, these data are further presented in an ENPOLITE-style plot [Fig. 6(b)] as described in [26], which additionally demonstrates increasing power capability and cyclability over subsequent cell generations. Interestingly, a decrease in both the used specific power and used specific energy parameters is observed between cell types A and B. This decrease coincides with the change from one to two jelly rolls inside the PHEV2-size casing (Fig. 1) and a decrease in the nominal cell voltage (Table I). Whether causal or not, these changes for cell type B coincide with greatly improved cyclability (Figs. 2 and 6). Any such shortcomings were soon resolved, as cell type C exhibits improved performance and cyclability by all metrics. One design change for cell type C was the shift from vertical winding to horizontal winding (Fig. 1). This leads to more efficient packing of the jelly rolls inside the can and improved volumetric energy density. This design feature is maintained for cell type D (not photographed).

Regarding DCIR, the linear relationship between capacity retention and DCIR rise seen for the early version of this cell size has evolved to a more complex nonmonotonic relationship. Due to this evolving relationship, the useful correlations

between DCIR and cell capacity from earlier generations are not applicable to more modern, energy-optimized cells. This may be a consequence of additives used to enhance shelf stability or cell performance. In any case, the increased complexity of DCIR data reveals an increasingly complex field of electrochemical phenomena within the cell and increases the difficulty of meaningful cell monitoring.

Many varied aging processes have been observed and identified in this work. Both early and more recent versions of the PHEV2-format cells show tendencies of swelling toward EOL, especially at higher (3C) charging currents. Such swelling can be due to expansion of the solid-phase electrode materials as well as gas generation from breakdown of the liquid electrolyte. Cell type A shows more severe aging of the NMC111 material than the graphite when cycled at slower charging currents. However, the graphite seems to be more affected by cycling at higher charging currents. When compared to cell types B and C, which in turn show no severe loss of active material, it appears that optimizations have been implemented to improve the performance and longevity of both electrodes. All three cell types also show loss of cyclable lithium upon cycling, both at slow and fast charging currents. One possible explanation of the different aging behaviors between cell types could be that different rates of loss of cyclable lithium affect the final outcome of electrode active material loss at EOL [27]. In some cases, loss of cyclable lithium by formation of solid-electrolyte interphase could help to passivate certain mechanisms and hold particles together. However, after a certain amount lost, local overpotentials could increase to the point that lithium plating [28] or other catastrophic mechanisms are induced. One such mechanism could be electrode dry out due to long-term electrolyte degradation [3], [20]. In this way, the internal electrochemical environment is dynamic and changing with age of the cell. A hypothesis regarding the difference in cyclability between the cell generations could be correlated with the homogeneity of lithium distribution in the anode, a homogeneity that can decrease during especially shallow cycle aging, shown by Lewerenz and Sauer [29] on automotive-grade prismatic 25-Ah cells. In addition, there could be a difference in immobilized lithium plating between the cell generations in the 3C-charging case. We showed in an earlier publication that we indeed obtained lithium plating when cycling cell type A at a 3C-charging current [3]. According to Epding *et al.* [9], this type of immobilized lithium plating is recoverable to some extent if sufficient rest is applied between cycles, which was shown for automotive-grade prismatic 25-Ah cells. This type of needed rest was not applied in our tests, and one hypothesis could hence be that this mechanism is valid for cell type A, while it has been mitigated in the later cell generations.

The changing mechanisms of passivation and aging could contribute to the fitted changes in CE during the life of a cell. For each cell type, the initial CE appears to be similar for both slow charging and fast charging. When cycling with high charging currents, a constant CE is seen until EOL; in some cases, there is a shift to sudden fade (decreased CE) close to EOL. When cycling with low charging currents, the initial low CE improves after a few 100 equivalent full cycles, sometimes in several steps. This decelerated aging behavior is well known for lithium-ion batteries but still hard to predict, especially if it is followed by a sudden fade as seen in other work [30]. Due to these shifting regimes, it is difficult to recommend CE measurements as a BOL screening technique to extrapolate to EOL as there are cases where this type of extrapolation could either overestimate or underestimate battery lifetime. Regarding the test cases in this study, CE measurements at the beginning of the test could have been useful for predicting aging of the cells cycled with the 3C charging regime, but they would have severely underestimated lifetime for cells cycled with the 1C charging regime. Furthermore, the accuracy and relevance of CE measurements are greatly affected by the temperature and charge rate of each test [31]. We suggest rather that such measurements may be used first to identify defective cells and then at intermittent check-ups to identify which aging regime a battery is in. By tracking a history of CE over the life of a battery, we may be able to develop stronger short-term predictions of cyclability and understand what triggers these observed changes in the aging regime.

V. Conclusion

We have compared three different lithium-ion battery cell generations of the prismatic VDA-standard PHEV2 regarding lifetime, with a focus on usage in electrified heavy-duty vehicles. The energy density has increased by almost 50% over a four-year period and three cell generations, while the specific energy has increased by a more moderate 18%. The equivalent full-cycle throughput, under 1C/1C charge/discharge in a 20%–80% SOC window and at +35 °C, is also much improved through cell generations while a more moderate increase in cyclability at 3C/1C is seen. The DCIR behavior changes throughout the cell generations from a linear relationship with capacity retention to a nonmonotonic one, complicating strategies for the monitoring of cell health. Despite this monitoring challenge, modern versions of the VDA PHEV2 cell format offer almost 50-Ah capacity, which means an impressively doubled capacity in eight years. These observed improvements are all independent of cell chemistry and format and can be attributed to more subtle developments in cell internal design and production for the latest generations of automotive-grade prismatic cells. Altogether, the results from this study point out that the VDA PHEV2 cell format remains a viable choice for electrified heavy-duty vehicles such as inner-city distribution PHEV trucks or even BEVs.

Acknowledgment

The authors would like to thank all industrial and academic participants from the consortium for their contributions throughout the various projects. The cycling was carried out within the Batterifonden Project Fast-Charging of Large Energy optimized Li-ion Cells for Electrified Drivelines (Grant number: 40501-1) and the Energy Efficient Vehicles Program Project Electrochemical Study of durability aspects in large vehicle batteries (Grant number: 30770-1) and could be realized through the Batterifonden Project Aging of Lithium-Ion Battery Cells with Nickel-rich Cathodes for Electromobility (ALINE) (Grant number: 45538-1).

REFERENCES

[1] M. Klett *et al.*, "Non-uniform aging of cycled commercial $LiFePO_4$//graphite cylindrical cells revealed by post-mortem analysis," *J. Power Sources*, vol. 257, pp. 126–137, Jul. 2014, doi: 10.1016/j.jpowsour.2014.01.105.

[2] M. Klett *et al.*, "Uneven film formation across depth of porous graphite electrodes in cycled commercial Li-ion batteries," *J. Phys. Chem. C*, vol. 119, no. 1, pp. 90–100, Jan. 2015, doi: 10.1021/jp509665e.

[3] A. S. Mussa *et al.*, "Fast-charging effects on ageing for energy-optimized automotive $LiNi_{1/3}Mn_{1/3}Co_{1/3}O_2$/graphite prismatic lithium-ion cells," *J. Power Sources*, vol. 422, pp. 175–184, May 2019, doi: 10.1016/j.jpowsour.2019.02.095.

[4] U. Mattinen, M. Klett, G. Lindbergh, and R. W. Lindström, "Gas evolution in commercial Li-ion battery cells measured by on-line mass spectrometry—Effects of C-rate and cell voltage," *J. Power Sources*, vol. 477, Nov. 2020, Art. no. 228968, doi: 10.1016/j.jpowsour.2020.228968.

[5] A. Gailani, R. Mokidm, M. El-Dalahmeh, M. El-Dalahmeh, and M. Al-Greer, "Analysis of lithium-ion battery cells degradation based on different manufacturers," in *Proc. 55th Int. Universities Power Eng. Conf. (UPEC)*, Sep. 2020, pp. 1–6, doi: 10.1109/UPEC49904.2020.9209759.

[6] Y. Olofsson, J. Groot, T. Katrašnik, and G. Tavčar, "Impedance spectroscopy characterisation of automotive NMC/graphite Li-ion cells aged with realistic PHEV load profile," in *Proc. IEEE IEVC*, Dec. 2014, pp. 1–6, doi: 10.1109/IEVC.2014.7056095.

[7] J. Schmitt *et al.*, "Measurement of gas pressure inside large-format prismatic lithium-ion cells during operation and cycle aging," *J. Power Sources*, vol. 478, Dec. 2020, Art. no. 228661, doi: 10.1016/j.jpowsour.2020.228661.

[8] A. Bessman, R. Soares, O. Wallmark, P. Svens, and G. Lindbergh, "Aging effects of AC harmonics on lithium-ion cells," *J. Energy Storage*, vol. 21, pp. 741–749, Feb. 2019, doi: 10.1016/j.est.2018.12.016.

[9] B. Epding, B. Rumberg, H. Jahnke, I. Stradtmann, and A. Kwade, "Investigation of significant capacity recovery effects due to long rest periods during high current cyclic aging tests in automotive lithium ion cells and their influence on lifetime," *J. Energy Storage*, vol. 22, pp. 249–256, Apr. 2019, doi: 10.1016/j.est.2019.02.015.

[10] *Industry Review of xEV Battery Size Standards*, B.C.S.S. Committee, SAE International, Warrendale, PA, USA, Jun. 2018, doi: 10.4271/J3124_201806.

[11] T. Waldmann *et al.*, "A direct comparison of pilot-scale Li-ion cells in the formats PHEV1, pouch, and 21700," *J. Electrochem. Soc.*, vol. 168, no. 9, Sep. 2021, Art. no. 090519, doi: 10.1149/1945-7111/ac208c.

[12] E. Schaltz, D.-I. Stroe, K. Norregaard, B. Johnsen, and A. Christensen, "Partial charging method for lithium-ion battery state-of-health estimation," in *Proc. 14th Int. Conf. Ecol. Vehicles Renew. Energies (EVER)*, May 2019, pp. 1–5, doi: 10.1109/EVER.2019.8813645.

[13] A. S. Mussa, G. Lindbergh, M. Klett, P. Gudmundson, P. Svens, and R. W. Lindström, "Inhomogeneous active layer contact loss in a cycled prismatic lithium-ion cell caused by the jelly-roll curvature," *J. Energy Storage*, vol. 20, pp. 213–217, Dec. 2018, doi: 10.1016/j.est.2018.09.012.

[14] A. J. Smith, J. C. Burns, S. Trussler, and J. R. Dahn, "Precision measurements of the Coulombic efficiency of lithium-ion batteries and of electrode materials for lithium-ion batteries," *J. Electrochem. Soc.*, vol. 157, no. 2, p. A196, 2010, doi: 10.1149/1.3268129.

[15] I. Bloom, L. K. Walker, J. K. Basco, D. P. Abraham, J. P. Christophersen, and C. D. Ho, "Differential voltage analyses of high-power lithium-ion cells. 4. Cells containing NMC," *J. Power Sources*, vol. 195, no. 3, pp. 877–882, 2010, doi: 10.1016/j.jpowsour.2009.08.019.

[16] A. J. Smith, J. C. Burns, X. Zhao, D. Xiong, and J. R. Dahn, "A high precision coulometry study of the SEI growth in Li/graphite cells," *J. Electrochem. Soc.*, vol. 158, no. 5, p. A447, 2011, doi: 10.1149/1.3557892.

[17] T. S. Pathan, M. Rashid, M. Walker, W. D. Widanage, and E. Kendrick, "Active formation of Li-ion batteries and its effect on cycle life," *J. Phys., Energy*, vol. 1, no. 4, Oct. 2019, Art. no. 044003, doi: 10.1088/2515-7655/ab2e92.

[18] M. Dubarry, V. Svoboda, R. Hwu, and B. Y. Liaw, "Incremental capacity analysis and close-to-equilibrium OCV measurements to quantify capacity fade in commercial rechargeable lithium batteries," *Electrochem. Solid-State Lett.*, vol. 9, no. 10, p. A454, 2006, doi: 10.1149/1.2221767.

[19] P. Svens, R. Eriksson, J. Hansson, M. Behm, T. Gustafsson, and G. Lindbergh, "Analysis of aging of commercial composite metal oxide—$Li_4Ti_5O_{12}$ battery cells," *J. Power Sources*, vol. 270, pp. 131–141, Dec. 2014, doi: 10.1016/j.jpowsour.2014.07.050.

[20] D. A. Stevens, R. Y. Ying, R. Fathi, J. N. Reimers, J. E. Harlow, and J. R. Dahn, "Using high precision coulometry measurements to compare the degradation mechanisms of NMC/LMO and NMC-only automotive scale pouch cells," *J. Electrochem. Soc.*, vol. 161, no. 9, pp. A1364–A1370, 2014, doi: 10.1149/2.0971409jes.

[21] C. Pastor-Fernández, K. Uddin, G. H. Chouchelamane, W. D. Widanage, and J. Marco, "A comparison between electrochemical impedance spectroscopy and incremental capacity-differential voltage as Li-ion diagnostic techniques to identify and quantify the effects of degradation modes within battery management systems," *J. Power Sources*, vol. 360, pp. 301–318, Aug. 2017, doi: 10.1016/j.jpowsour.2017.03.042.

[22] A. J. Smith, P. Svens, M. Varini, G. Lindbergh, and R. W. Lindström, "Expanded *in situ* aging indicators for lithium-ion batteries with a blended NMC-LMO electrode cycled at sub-ambient temperature," *J. Electrochem. Soc.*, vol. 168, no. 11, Nov. 2021, Art. no. 110530, doi: 10.1149/1945-7111/ac2d17.

[23] B. Stiaszny, J. C. Ziegler, E. E. Krauß, M. Zhang, J. P. Schmidt, and E. Ivers-Tiffée, "Electrochemical characterization and post-mortem analysis of aged $LiMn_2O_4$–NMC/graphite lithium ion batteries—Part II: Calendar aging," *J. Power Sources*, vol. 258, pp. 61–75, Jul. 2014, doi: 10.1016/j.jpowsour.2014.02.019.

[24] N. Yabuuchi and T. Ohzuku, "Novel lithium insertion material of $LiCo_{1/3}Ni_{1/3}Mn_{1/3}O_2$ for advanced lithium-ion batteries," *J. Power Sources*, vols. 119–121, pp. 171–174, Jul. 2003, doi: 10.1016/S0378.7753(03)00173 3.

[25] *3.7V 50Ah NCM Prismatic Li-Ion Battery Cell for EV*. Osn Power. Accessed: Jun. 11, 2021. [Online]. Available: https://www.osnpower.com/3-7v-50ah-ncm-prismatic-li-ion-battery-cell-for-ev_p39.html

[26] P. Dechent *et al.*, "ENPOLITE: Comparing lithium-ion cells across energy, power, lifetime, and temperature," *ACS Energy Lett.*, vol. 6, no. 6, pp. 2351–2355, Jun. 2021, doi: 10.1021/acsenergylett.1c00743.

[27] Q. Zhang and R. E. White, "Capacity fade analysis of a lithium ion cell," *J. Power Sources*, vol. 179, no. 2, pp. 793–798, May 2008, doi: 10.1016/j.jpowsour.2008.01.028.

[28] T. C. Bach *et al.*, "Nonlinear aging of cylindrical lithium-ion cells linked to heterogeneous compression," *J. Energy Storage*, vol. 5, pp. 212–223, Feb. 2016, doi: 10.1016/j.est.2016.01.003.

[29] M. Lewerenz and D. U. Sauer, "Evaluation of cyclic aging tests of prismatic automotive $LiNiMnCoO_2$-graphite cells considering influence of homogeneity and anode overhang," *J. Energy Storage*, vol. 18, pp. 421–434, Aug. 2018, doi: 10.1016/j.est.2018.06.003.

[30] T. Waldmann, B.-I. Hogg, and M. Wohlfahrt-Mehrens, "Li plating as unwanted side reaction in commercial li-ion cells—A review," *J. Power Sources*, vol. 384, pp. 107–124, Apr. 2018, doi: 10.1016/j.jpowsour.2018.02.063.

[31] J. C. Burns, D. A. Stevens, and J. R. Dahn, "*In-situ* detection of lithium plating using high precision coulometry," *J. Electrochem. Soc.*, vol. 162, no. 6, pp. A959–A964, 2015, doi: 10.1149/2.0621506jes.

Pontus Svens received the Ph.D. degree in chemical engineering from the KTH Royal Institute of Technology, Stockholm, Sweden, in 2014.

From 2008 to 2018, he worked as a Lithium-Ion Battery Specialist in vehicle electrification with Scania CV AB, Södertälje, Sweden. Since 2016, he has been holding an affiliated faculty position in the fields of lithium-ion batteries and fuel cells with the Applied Electrochemistry Research Group, KTH Royal Institute of Technology. He is currently working as a Senior Scientist in the field of electrochemical energy converters with Scania CV AB.

Alexander J. Smith received the B.S.E. degree in chemical and biomolecular engineering from the University of Pennsylvania, Philadelphia, PA, USA, in 2015, and the M.Sc. degree in chemical engineering for energy and environment from the KTH Royal Institute of Technology, Stockholm, Sweden, in 2018, where he is currently pursuing the Ph.D. degree in chemical engineering with a research focus on developing tools for characterizing aging in lithium-ion batteries.

Jens Groot received the Ph.D. degree from the Chalmers University of Technology, Gothenburg, Sweden, with a focus on high-power Li-ion battery lifetime prediction and modeling, in 2014.

From 2003 to 2020, he was an Energy Storage Specialist with the Volvo Group Trucks Technology, Gothenburg, working in research and development for heavy-duty vehicles with a focus on battery characterization, cycle life evaluation, and thermal and electrochemical modeling. Since 2021, he has been a Senior Strategic Battery Architect with Volvo Car Sverige AB, Gothenburg, and he recently changed his position to the Chief Engineer with Polestar Performance AB, Gothenburg.

Matthew J. Lacey received the Ph.D. degree from the University of Southampton, Southampton, U.K., in 2012.

From 2012 to 2019, he worked with the Ångström Advanced Battery Centre, Uppsala University, Uppsala, Sweden, first as a Post-Doctoral Researcher and then as a Permanent Member of Staff. He currently works on a variety of projects relating to the chemistry of electric vehicle batteries as a Development Engineer within materials technology at Scania CV AB, Södertälje, Sweden.

Göran Lindbergh received the M.Sc. and Ph.D. degrees from the KTH Royal Institute of Technology, Stockholm, Sweden, in 1985 and 1991, respectively.

Since 2003, he has been a Professor of chemical engineering with the KTH Royal Institute of Technology, where he is currently the Head of the Applied Electrochemistry Research Group, working with electrochemical power sources and electrolytic processes in the field of electrochemical engineering. A common theme in the ongoing research projects is the mathematical modeling and electrochemical characterization of electrochemical systems. Of special importance is the development and application of porous electrode theories for battery electrodes and gas diffusion fuel cell electrodes.

Rakel Wreland Lindström received the Ph.D. degree in inorganic chemistry from Gothenburg University, Gothenburg, Sweden, in 2003.

After completion of two postdocs periods with Paris-Tech, Paris, France, and University of Ulm, Ulm, Germany, she holds a faculty position with the KTH Royal Institute of Technology, Stockholm, Sweden. Since 2020, she has been a Full Professor in chemical engineering with the KTH Royal Institute of Technology. Over the years, her research has covered a wide range of electrochemical systems, including corrosion, fuel cells, and batteries with particular interest for *in situ* studies combining electrochemical methods with other analytical or microscopic techniques.